

PROCEEDINGS OF SPIE

[SPIDigitalLibrary.org/conference-proceedings-of-spie](https://spiedigitallibrary.org/conference-proceedings-of-spie)

Comparative steady-state and time-resolved emission spectroscopy of Mn-doped CsPbCl₃ perovskite nanoparticles and bulk single crystals for photonic applications

Hömmerich, U., Barnett, J., Kabir, A., Ghebreyessus, K., Hampton, K., et al.

U. Hömmerich, J. Barnett, A. Kabir, K. Ghebreyessus, K. Hampton, S. Uba, I. Uba, D. Geddis, C. Yang, S. B. Trivedi, S. Fraden, Ali Aghvami, "Comparative steady-state and time-resolved emission spectroscopy of Mn-doped CsPbCl₃ perovskite nanoparticles and bulk single crystals for photonic applications," Proc. SPIE 11682, Optical Components and Materials XVIII, 116821J (5 March 2021); doi: 10.1117/12.2582217

SPIE.

Event: SPIE OPTO, 2021, Online Only

Comparative steady-state and time-resolved emission spectroscopy of Mn doped CsPbCl₃ perovskite nanoparticles and bulk single crystals for photonic applications

U. Hömmerich^{a*}, J. Barnett^a, A. Kabir^a, K. Ghebreyessus^a, K. Hampton^a, S. Uba^a, I. Uba^a, D. Geddis^a, C. Yang^b, S. B. Trivedi^b, S. Fraden^c, and Ali Aghvami^c

^aHampton University, Hampton, VA 23668; ^bBrimrose Technology Corporation, Sparks Glencoe, MD 21152, ^cBrandeis University, Waltham, MA 02453

ABSTRACT

Manganese doped inorganic halide perovskites continue to be of current interest for applications in light emitting devices and down-converters in solar cells. In this work we prepared Mn doped CsPbCl₃ (Mn: CPC) bulk crystals and nanoparticles (NPs) and compared their emission properties. Bulk crystals were grown from the melt by vertical Bridgman technique and NPs were synthesized using a microwave assisted method. Under ultraviolet excitation at 350 nm, bulk crystal and NPs exhibited a broad orange emission centered in the ~600 nm range at room temperature. The broadband emission was assigned to the intra-3d transition ⁴T₁ → ⁶A₁ of Mn²⁺ ions incorporated in the CPC host lattice. The Mn²⁺ emission lifetimes were nearly exponential with values of 1.1 ms for NPs and 0.7 ms for the bulk crystal. NPs also showed exciton emission peaking at ~402 nm, whereas the bulk crystal exhibited no emission near the band-edge. Instead, the bulk material revealed a weak below-gap emission in the 450-550 nm region suggesting the existence of defect states. The excitation spectra for the orange Mn²⁺ emission from NPs and bulk crystals of Mn: CPC were significantly different indicating distinct excitation pathways. The excitation spectrum of the orange Mn²⁺ emission from NPs showed excitonic structure similar to the absorption spectrum suggesting an efficient energy transfer from excitons to Mn²⁺ ions. In contrast, UV excitation was less efficient for the bulk crystal and the excitation was dominated by below-gap excitation bands centered at 427 and 500 nm.

Keywords: Halide perovskites, Mn²⁺ Spectroscopy, visible light sources

1. INTRODUCTION

The development of cesium lead halide perovskites nanoparticles (NPs) with composition CsPbX₃ (X=Cl, Br, I) continues to be of great current interest for optoelectronic applications including light emitting devices and solar cells [1-5]. High emission quantum yields have been reported for CsPbX₃ NPs in conjunction with narrow emission bands covering the entire visible spectral region. The emission wavelengths of CsPbX₃ NPs can be color tuned through varying halide composition or quantum confinement effects. For example red emission can be obtained from CsPbI₃ nanoparticles, but emission efficiency and material instability remain critical issues [6]. Besides compositional tuning of halide perovskites, visible and IR emission wavelengths can also be achieved through doping of transition metal and/or rare earth ions [7-10]. Most suitable for metal doping is CsPbCl₃ with a wide band gap of ~3 eV and exciton emission at ~410 nm. Adding Mn²⁺ ions as dopants into CsPbCl₃ results into bright orange emission, which can be assigned to the ⁴T₁→⁶A₁ transition of tetrahedrally coordinated Mn²⁺ ions [11-16]. In this work, the optical properties of Mn: CPC nanoparticles and bulk crystals were compared to gain better understanding of the excitation and de-excitation processes for possible applications in photonic devices. Nanoparticles were prepared by a microwave assisted method and single crystals were grown from the melt by vertical Bridgman technique. All Mn: CPC samples revealed broad emission bands centered at ~605 nm under ultra-violet excitation with emission lifetimes in the millisecond range at room-temperature. Excitation wavelengths and temperature dependent emission studies revealed significant differences in the Mn²⁺ excitation and de-excitation pathways of Mn: CPC nanoparticles compared to bulk single crystals.

* corresponding author: uwe.hommerich@hamptonu.edu

2. MATERIAL PREPARATION AND EXPERIMENTAL DETAILS

For the synthesis of Mn doped CPC NPs, a microwave reaction tube with a volume of 35 mL was used as a reaction vessel. The specific instrument was a Discover-CEM research grade microwave reactor with 250 PSI pressure and 200 W power operating parameters. In a typical experiment, PbCl_2 (0.400 mmol), MnCl_2 (0.80 mmol), 1-octadecene (10 mL), oleic acid (1 mL), oleylamine (1 mL) and trioctylphosphine oxide (0.50 g) were loaded into the microwave tube and stirred at 80°C for 1 h under purging nitrogen flow. To improve the solubility of PbCl_2 , 2.0 mL of trioctylphosphine was added as a co-solvent. After complete solubilization of PbCl_2 , cesium acetate (0.10 mmol) powder was added and the reaction mixture was placed in the microwave reactor and heated to the desired temperature. The reaction temperature was set to 160°C and the reaction duration time was 10 min. After completion of the reaction, the mixture was cooled to room temperature. The Mn doped CPC nanocrystals were extracted from the crude reaction mixture by adding 10 mL of hexane and centrifuging for 10 min. After centrifugation, the supernatant was discarded and the nanocrystals were redispersed in 10 mL of hexane and then centrifuged for 10 min. Drop-casted films of Mn: CPC NPs with $\sim 6\ \mu\text{m}$ thickness were used for optical spectroscopy. The bulk crystal of Mn: CPC was grown by a vertical Bridgman technique using a two-zone furnace [10]. Mn: CPC ($\sim 2\ \text{wt}\%$) was synthesized from high purity starting materials of CsCl, PbCl_2 , and MnCl_2 loaded inside a pre-cleaned quartz ampoule. The material was then heated to $\sim 110^\circ\text{C}$ under a dynamic vacuum for 24 hours before vacuum sealing. For crystal growth experiments, the ampoule was positioned into the hot-zone of the growth furnace at $\sim 30\text{--}40^\circ\text{C}$ above the melting point for 24 hours. The growth ampoule was subsequently lowered at a growth speed of $\sim 2\ \text{mm/h}$. After the crystal growth was completed, the furnace was slowly cooled to room-temperature over a time period of three days. The Mn:CPC crystal exhibited an orange coloration indicating the incorporation of Mn^{2+} ions. A small sample disk with 2 mm thickness and 3-4 mm diameter was cut from the ingot and polished for spectroscopic studies. Transmission spectra were measured using a Shimadzu UV-3600 spectrophotometer. Emission spectra, excitation spectra, and lifetimes were recorded employing an Edinburgh Instruments FLS 980 fluorescence spectrometer.

3. RESULTS AND DISCUSSION

3.1 Results of NP synthesis, crystal growth and structural studies

Pictures of the synthesized colloidal Mn: CPC NPs solution and bulk crystal under ambient and UV light are shown in Fig 1. Under ambient conditions the NP solution was clear with a weak orange coloration, whereas the bulk crystal was translucent with a more pronounced orange color. Under UV excitation both samples exhibited an orange emission, which was significantly brighter from the NPs compared to the bulk crystal. The crystal structure of Mn: CPC was confirmed through XRD studies and the particle size of NPs was estimated to be $\sim 15\text{--}20\ \text{nm}$ from TEM images (Fig. 2).

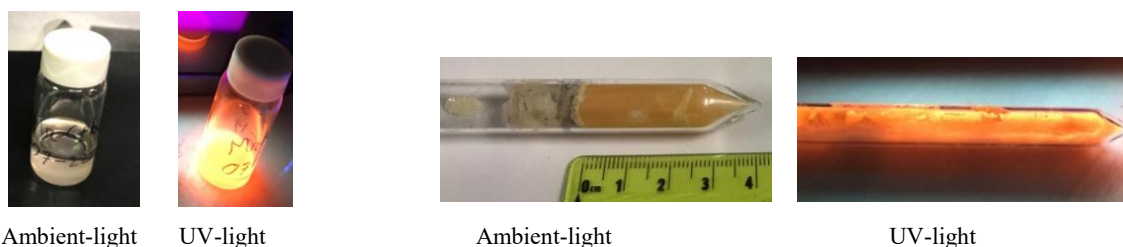


Figure 1. Pictures of Mn: CPC NPs colloidal solution (left) and bulk crystal (right) under ambient light and UV light.

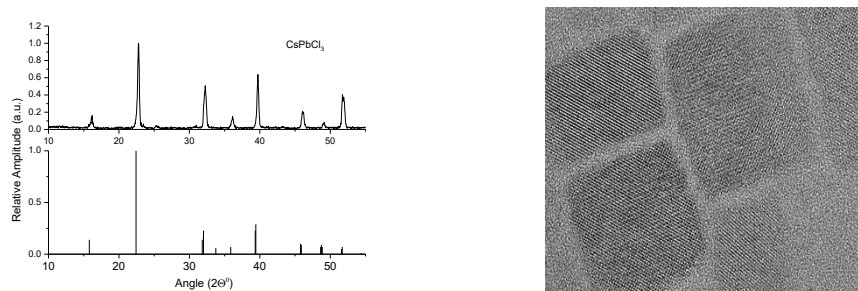


Figure 2. Powder XRD of Mn: CPC bulk crystal (left) and TEM image of Mn: CPC NPs (right).

3.2 Absorption, emission, and excitation spectroscopy at room-temperature

The absorption and emission spectra of Mn: CPC nanoparticles and bulk crystal are shown in Fig. 3. The band-edge energy was derived from tauc-plots and yielded values of ~ 396 nm (3.13 eV) for the NPs and ~ 430 nm (2.89 eV) for the bulk crystal [16,17]. Under UV excitation (350 nm), the Mn: CPC NPs showed excitonic emission peaking at ~ 403 nm (FWHM: 16 nm) and a broad Mn^{2+} emission centered at ~ 606 nm (FWHM: 88 nm). The peak intensity ratio of Mn^{2+} to exciton emission was $\sim 15:1$. The Mn: CPC bulk crystal showed a similar Mn^{2+} emission peaking at 602 nm with a bandwidth of 85 nm at FWHM. On the contrary to NPs, no exciton emission was observed from the bulk crystal, but some defect related broad band emission in the 420-550 nm range. The peak intensity ratio of Mn^{2+} to defect emission was $\sim 4:1$. For both NPs and bulk material of Mn: CPC the bright orange emission is ascribed to the spin-forbidden intra-3d transition ${}^4\text{T}_1 \rightarrow {}^6\text{A}_1$ of octahedrally coordinated Mn^{2+} ions in the CPC host lattice.

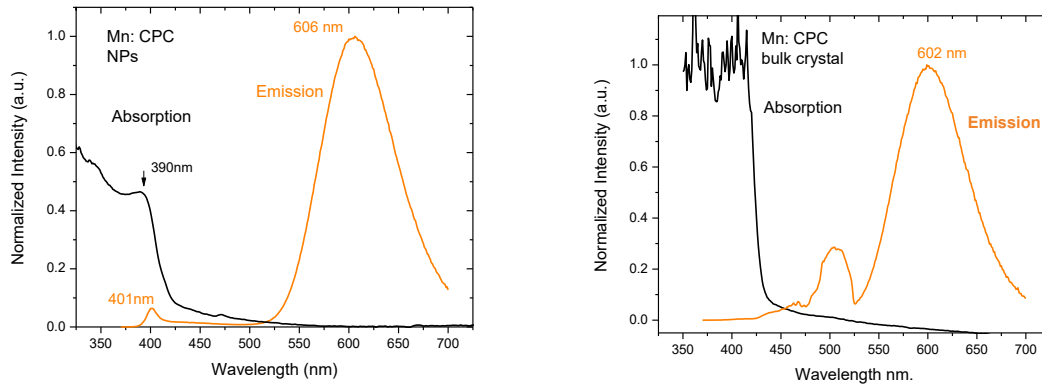


Figure 3: Room temperature absorption and emission spectra for Mn: CPC nanoparticles (left) and Mn: CPC bulk crystal (right). The emission was excited with 350 nm UV light.

The normalized excitation spectra of the investigated Mn: CPC samples are shown in Fig. 4. The signal was monitored at the peak wavelength of the orange Mn^{2+} emission (~ 605 nm). The excitation spectrum of NPs showed an excitonic structure at ~ 385 nm followed by a continuous excitation extending to shorter UV wavelengths. The excitation spectrum exhibited similar excitonic features as observed in the absorption spectrum of NPs (Fig 3), which provides evidence for an efficient energy transfer from exciton states to Mn^{2+} ions. Weak below-gap excitation bands were observed in the 410-450 nm suggesting defect related excitation pathways and possibly weaker underlying intra-3d absorption bands of Mn^{2+} ions. The excitation spectrum for the bulk crystal was significantly different and showed distinct below-gap excitation bands centered at 427 nm and 500 nm. Based on comparison to published data [18], these bands are tentatively assigned to the intra-3d transitions ${}^6\text{A}_1 \rightarrow {}^4\text{A}_1({}^4\text{G})$, ${}^4\text{E}({}^4\text{G})$ (425 nm band) and ${}^6\text{A}_1 \rightarrow {}^4\text{T}_1({}^4\text{G})$, (510 nm band). Weaker Mn^{2+} excitation bands were observed above the band-gap of CPC, which indicates that orange emission from the bulk crystal can also be excited at UV wavelength through carrier-mediated processes.

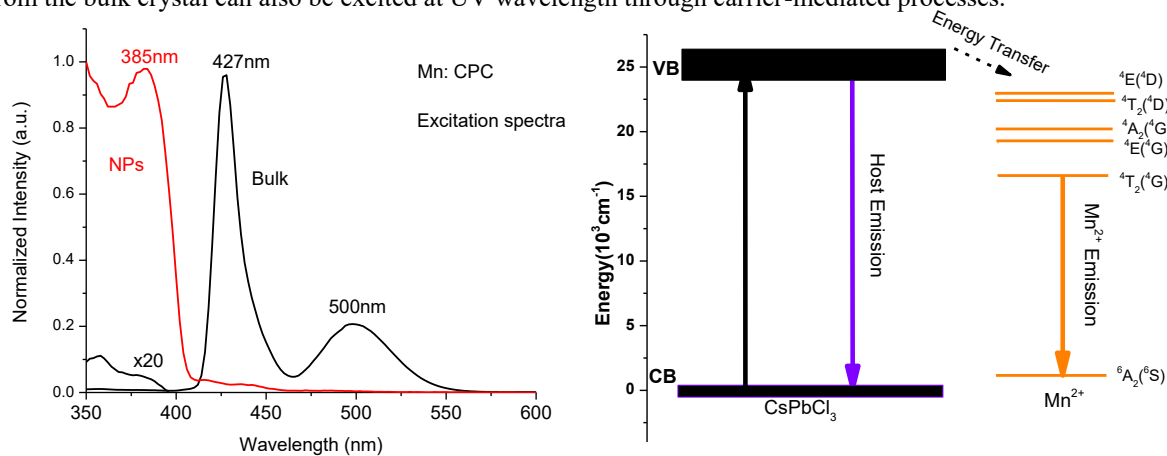


Figure 4: Room temperature excitation spectra of Mn: CPC bulk crystal and NPs. The emission was monitored at a wavelength of ~ 605 nm for both excitation scans.

The emission decay curves for Mn: CPC NPs and bulk crystal under UV excitation (350 nm) are shown in Fig. 5. The Mn^{2+} emission lifetimes were nearly exponential in NPs and bulk crystal with values of 1.1 ms and 0.7 ms, respectively. The single exponential nature of emission lifetimes indicates a nearly homogenous environment for Mn^{2+} ions incorporated in the CPC lattice. For the bulk crystal, the emission was also excited using excitation wavelengths matching the strong below-gap excitation bands at ~ 420 nm and ~ 530 nm. No significant differences in lifetimes were observed for above and below-gap excitation suggesting that the same class of Mn^{2+} ions are optically excited independent of excitation pathway. The initial rise-time in the decay curve under 532 nm pumping possibly indicates energy transfer from mid-gap defect states into the Mn^{2+} intra-3d excited state.

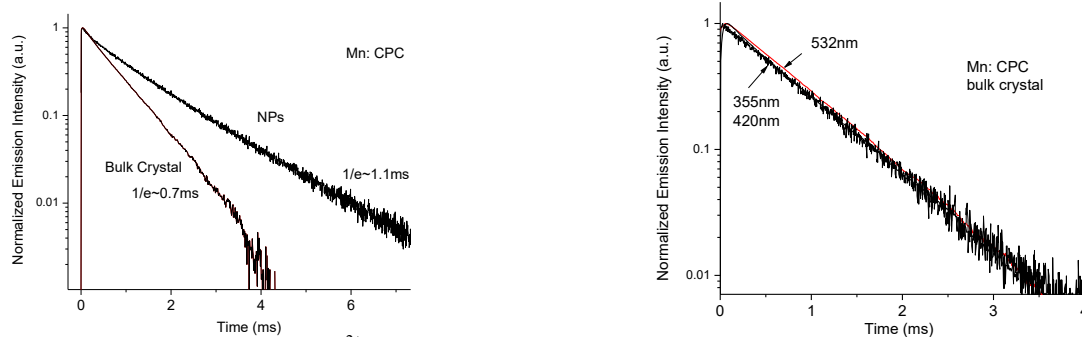


Figure 5: Comparison of the Mn^{2+} emission decay curves for NPs and bulk crystal of Mn: CPC under UV pumping (left). Emission decay curves under 355, 425, and 532 nm excitation for the bulk crystal of Mn: CPC (right).

3.3 Temperature dependent emission spectroscopy

Temperature dependent emission spectra for Mn: CPC NPs and bulk crystals are shown Fig. 6. The emission spectra were excited using 350 nm optical pumping. At room temperature the dominant spectral feature is a broad Mn^{2+} emission peaking at ~ 600 -610 nm, whereas at 77 K strong exciton emission in the 400 nm range can be observed from both samples.

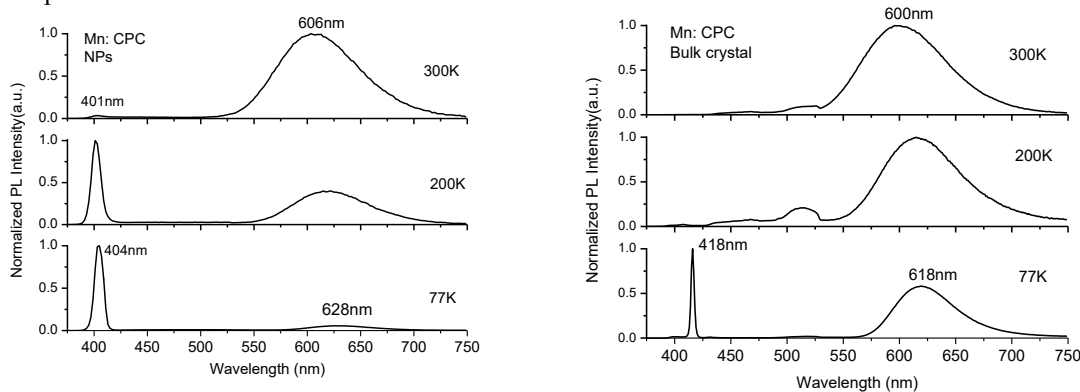


Figure 6: Normalized emission spectra of Mn: CPC NPs (left) and Mn: CPC crystal (right) at 77 K, 200 K and 300K.

For NPs and bulk crystal of Mn: CPC it was noticed that the intensity ratio of exciton to Mn^{2+} emission changed significantly when cooling the sample from 300 K to 77 K. For NPs at 300 K the broad Mn^{2+} emission centered at ~ 606 nm dominated the spectrum, whereas at 77 K the exciton emission at ~ 404 nm was the most intense emission feature. A similar observation was made for the Mn: CPC bulk crystal with the main difference that at 77 K the Mn^{2+} emission still exhibited a nearly equal intensity compared to the exciton peak. Following an initial fast decrease of exciton and Mn^{2+} emission in the range 77–150 K, an inverse temperature correlation between exciton and Mn^{2+} emission intensity was noticed from 150-300 K (Fig. 7). The exciton emission intensity continued to decrease until 300 K, whereas the Mn^{2+} emission increased significantly. This inverse temperature dependence behavior reflects on the energy transfer process from excitonic states to the ${}^4\text{T}_1$ Mn^{2+} excited state. As discussed in the literature for Mn: CPC NPs, this process is thermally activated and therefore strongly temperature dependent [15,19]. It has been reported before that hybrid lead halide perovskites NPs possess higher exciton binding energies compared to their bulk crystal counterparts leading to higher exciton emission at room-temperature [19]. Similar argument can be made here for Mn: CPC NPs versus bulk crystal. Compared to the bulk crystal, the exciton emission from the Mn: CPC NPs exhibited a higher temperature

stability, which results in a higher Mn^{2+} excitation efficiency and stronger orange emission at room-temperature under UV excitation.

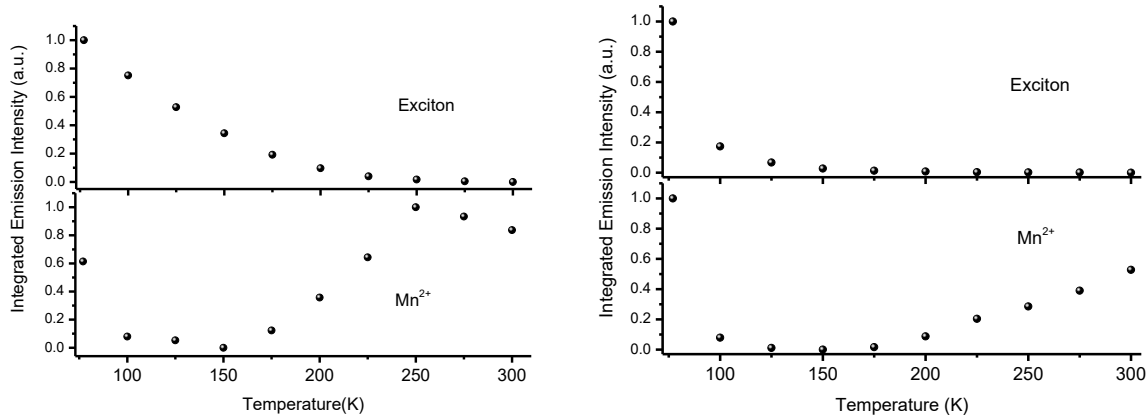


Figure 7: Temperature dependence of the integrated intensity of exciton and Mn^{2+} emissions for Mn: CPC NPs (left) and Mn: CPC crystal (right).

It can also be observed from Fig.6, that the Mn^{2+} emission blue-shifts by ~ 22 nm with increasing temperature, whereas the exciton emission blue-shifts by only ~ 0.5 nm for the same temperature range [20]. The large Mn^{2+} emission shift reflects on the strong sensitivity of the octahedrally coordinated Mn^{2+} ions to the surrounding crystal field environment. More specifically, the blue-shift of Mn^{2+} emission with increasing temperature relates to the decrease in crystal-field strength with the thermal expansion of the host lattice. According to the $3d^5$ Tanabe-Sugano diagram, the weaker crystal field (smaller Dq parameter) leads to a larger energy splitting and consequently a larger transition energy and blue shift of the emission band [20].

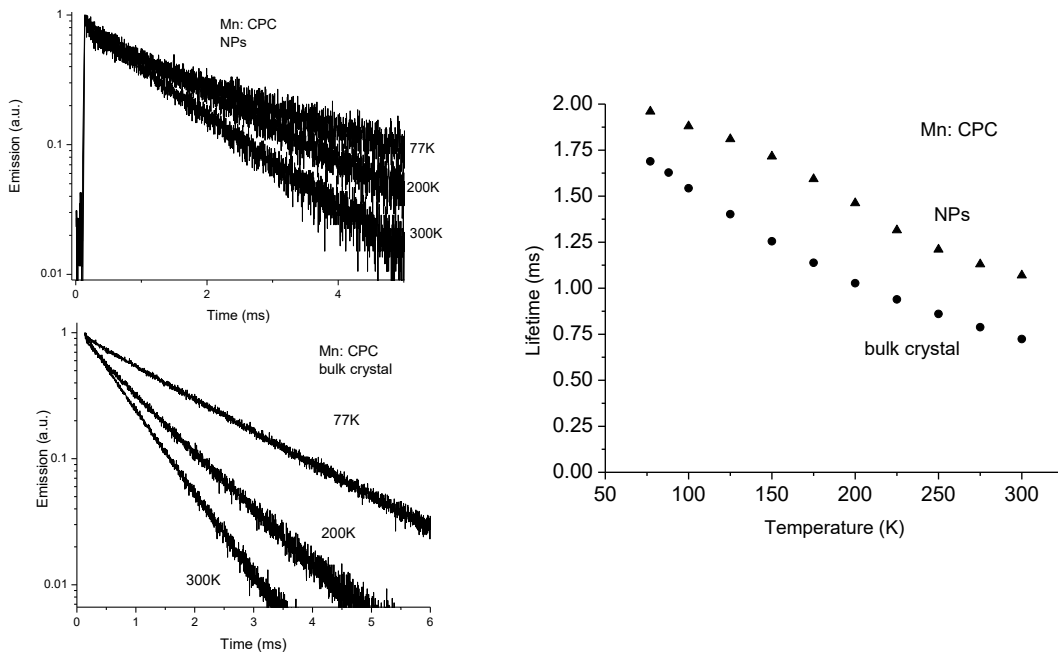


Figure 8: Temperature dependent Mn^{2+} emission decay curves (left) and exponential lifetime values (right) for Mn: CPC NPs and bulk crystal under 350 nm UV excitation.

The decay curves and lifetimes of Mn^{2+} ions for NPs and bulk crystal at different temperatures under above-gap excitation are shown in Fig 8. At 77 K the NPs lifetime was ~ 2.0 ms compared to ~ 1.7 ms for the bulk crystal. In both cases the lifetime decreased at higher temperatures leading to lifetime values at 300K of ~ 1.1 ms for NPs and ~ 0.7 ms

for the bulk crystal, respectively. The temperature change in lifetime is most likely due to non-radiative decay due to multi-phonon relaxations within the intra-3d Mn^{2+} transition or through energy-transfer processes to other defects/impurities [20]. Under the assumption that the 77 K lifetime is the purely radiative lifetime (τ_{rad}) the Mn^{2+} emission quantum efficiency (QE) was derived from the relation $\text{QE}=\tau_{300\text{K}}/\tau_{77\text{K}}$ [20] to be ~55% for NPs and ~41% for the bulk crystal. The QE for the NPs was also determined using an integration sphere method yielding a value of ~50%. The obtained QE values are in good agreement with published data on Mn: CPC NPs prepared by other methods with highest values ranging from 54-67% [11,21]. The QE of the bulk Mn: CPC crystal was slightly lower compared to the NPs but can be further optimized through additional purification studies of raw materials.

4. SUMMARY

Spectral and time-resolved emission studies were performed on Mn doped CsPbCl_3 nanoparticles and a bulk crystal as a function of temperature. The bulk crystal was grown from the melt by vertical Bridgman technique and NPs were synthesized using a microwave assisted method. Under UV optical excitation the samples showed bright orange emission centered at ~600 nm from Mn^{2+} ions (${}^4\text{T}_1 \rightarrow {}^6\text{A}_1$ transition) incorporated into the CsPbCl_3 lattice structure. The NPs of Mn: CPC showed also weak exciton emission at 300 K, whereas the bulk crystal exhibited broad-defect emission in the 400-550 nm range. It was observed that the Mn^{2+} emission from the bulk crystal was significantly weaker for above-gap excitation compared to below-gap excitation into absorption bands centered at 427 nm and 500 nm. The below-gap excitation bands were most likely due to intra-3d Mn^{2+} transitions overlapped with possible defect levels in Mn: CPC. Temperature dependent spectral measurements from 77-300 K showed an initial fast decrease of exciton and Mn^{2+} emissions followed by an inverse temperature correlation of both emissions from 150-300 K. Whilst the exciton emission continued to decrease, the Mn^{2+} emission gained intensity at higher temperatures. This inverse temperature behavior reflects on the energy transfer process from excitonic states to the ${}^4\text{T}_1$ Mn^{2+} excited state. Similar to results reported for hybrid lead halide perovskites, excitons in Mn: CPC NPs exhibit a higher temperature stability compared to the bulk crystal leading to enhanced energy transfer and Mn^{2+} emission at room-temperature. The Mn^{2+} emission lifetimes of NPs and bulk crystal were nearly exponential and showed a slight decrease from 77 -300 K. The reduced lifetimes at room temperature indicated non-radiative decay processes which limit the emission quantum efficiencies to ~55% and ~41% for NPs and bulk crystal, respectively. Further purification studies of raw materials for bulk crystal growth of Mn: CPC are in progress to improve the emission quantum efficiency. This work has shown that the investigated NPs and bulk crystal of Mn: CsPbCl_3 can produce efficient orange emission from Mn^{2+} ions with distinct excitation schemes. Both materials have potential in light source development related to LEDs or phosphor applications.

ACKNOWLEDGEMENTS

The work at Hampton University was supported by through grants NSF PREM DMR-1827820, NSF MRSEC DMR-2011486, and ARO-W911NF1810447.

REFERENCES

- [1] R. Babu, L. Giribabu, S. P. Singh, "Recent Advances in Halide-Based Perovskite Crystals and Their Optoelectronic Applications", *Cryst. Growth Des.* 18, 2645 (2018).
- [2] H.H. Ma, M. Imran, Z. Dang, and Z. Hu; "Growth of Metal Halide Perovskite, from Nanocrystal to Micron-Scale Crystal: A Review"; *Crystals*, 8, 182 (2018).
- [3] C.K. Siu, J. Zhao, Y. Wang, D. Yangm X. Xu, S. Pan, S. F. Yu; "Lasing characteristics of single-crystalline CsPbCl_3 perovskite microcavities under multiphoton excitation", *J. Phys. D: Appl. Phys.* 50, 225101 (2017).
- [4] Z. Xiao, R. A. Kerner; L. Zhao; N.L. Tran, K.M. Lee, T.W Koh; G.D. Scholes, G. D.; B.P. Rand, "Efficient perovskite light-emitting diodes featuring nanometer-sized crystallites. *Nat. Photonics* 11, 108 (2017).
- [5] R. E. Beal, D. J. Slotcavage, T. Leitjens, A. R. Bowring, R. A. Belisle, W. H. Nguyen, G. F. Burkhard, E.T. Hoke, M. D. McGehee, "Cesium Lead Halide Perovskites with Improved Stability for Tandem Solar Cells", *J. Phys. Chem. Lett.* 7, 746 (2016).

- [6] D. Li, C. S. Chen, Y. H. Wu, Z. G. Zhu, W. Y. Shih, W. H. Shih, "Improving stability of cesium lead iodide perovskite nanocrystals by solutions surface treatment", *ACS Omega*, 5, 18013 (2020).
- [7] Y. Zhou, J. Chen, Z. Dang, and Z. Hu, "Metal-doped lead halide perovskites: synthesis, properties, and optoelectronic applications, *Chem. Mater.* 30 6589 (2018).
- [8] D. Zhou, D. Liu, G. Pan, X. Chen, D. Li, W. Xu, X. Bai, and H. Song, "Cerium and Ytterbium Codoped Halide Perovskite Quantum Dots: A Novel and Efficient Downconverter for Improving the Performance of Silicon Solar Cells", *Adv. Mater.* 29, 1704149 (2017).
- [9] G. Pan, X. Bai, D. Yang, X. Chen, P. Jing, S. Qu, L. Zhang, D. Zhou, J. Zhu, W. Xu, B. Dong, H. Song, "Doping Lanthanide into Perovskite Nanocrystals: Highly Improved and Expanded Optical Properties", *Nano Lett.* 17, 8005 (2017).
- [10] U. Hommerich, D. Uba, A. Kabir, S. Trivedi, C. Yang, E. Brown, "Visible emission studies of melt-grown Dy-doped CsPbCl₃ and KPb₂Cl₅ crystals", *Opt. Mat. Exp.* 10, 2011 (2020).
- [11] A. K. Guria, S. K. Dutta, S. D. Adhikari, N. Pradhan, "Doping Mn²⁺ in lead halide perovskite nanocrystals: success and challenges", *ACS Energy Lett.* 2, 1014 (2017).
- [12] C. C. Lin, K. Y. Xu, D. Wang, A. Meijerink, "Luminescent manganese-doped CsPbCl₃ perovskite quantum dots", *Sci. Rep.* 7, 45906 (2017).
- [13] S. Ye, J.Y. Sun, Y.H. Han, Y. T. Zhou, Q.Y. Zhang, "Confining Mn²⁺ doped lead halide perovskite in zeolite-y as ultrastable orange-red phosphor composites for white-light-emitting diodes, *ACS Appl. Mater. Interfaces* 10, 24656 (2018).
- [14] Q. Wang, X. Zhang, Z. Jin, J. Zhang, Z. Gao, Y. Li, S. F. Liu, "Energy-down-shift CsPbCl₃ quantum dots for boosting the efficiency and stability of perovskite solar cells", *ACS Energy Lett.* 2, 1479 (2017).
- [15] W. Wu, W. Liu, O. Wang, Q. Han, O. Yang, "Temperature-dependent photoluminescence of pure and Mn-doped CsPbCl₃ nanocrystals", *J. Alloys and Compounds* 787, 165 (2019).
- [16] N. Pandey, A. Kumar, S. Chakrabarti, "Investigation of the structural, electronic, and optical properties of Mn-doped CsPbCl₃: theory and experiment", *RSC Adv.* 9, 29556 (2019).
- [17] M. Sebastian, J. A. Peters, C.C. Stoumpos, J. Im, S.S. Kostina, Z. Liu, M.G. Kanatzidis, A. J. Freeman, and B. W. Wessels, "Exitonic emissions and above-band-gap luminescence in the single-crystal perovskite semiconductors CsPbBr₃ and CsPbCl₃, *Physical Review B* 92, 235210 (2015).
- [18] R. Cao, Y. Ran, X. Lv, L. Xu, H. Wan, Q. Hu, T. Chen, C. Cao "Tunable multicolor luminescent properties of Ca₈ZnLa(PO₄)₇: Ce³⁺, Mn²⁺ phosphor via efficient energy transfer", *J. Lumin.* 214, 116549 (2019).
- [19] H. C. Woo, J. W. Choi, J. Shin, S. H. Chin, M. H. Ann, C. L. Lee,"Temperature-dependent photoluminescence of CH₃NH₃PbBr₃ perovskite quantum dots and bulk counterparts" *J. Phys. Chem. Lett.* 9, 4066 (2018).
- [20] B. Henderson, G.F. Imbusch, *Optical Spectroscopy of Inorganic Solids* (Oxford, United Kingdom: Clarendon, 1989)
- [21] F. Sui, M. Pan, Z. Wang, M. Chen, W. Li, Y. Shai, W. Li, C. Yang, "Quantum yield enhancement of Mn-doped CsPbCl₃ perovskite nanocrystals as luminescent down-shifting layer for CIGS solar cells", *Solar Energy* 206, 473 (2020).